A Platinum Open Access Journal for Organic Chemistry

Paper

Free to Authors and Readers | DOAJ Seal | *Arkivoc* **2024** (3) 202412252

Investigating physicochemical properties of MgO catalysts for the gas phase conversion of glycerol

Karl Mugford, Louise R. Smith, Mark Douthwaite, Nicholas F. Dummer, David J. Willock, Graham J. Hutchings, and Stuart H. Taylor*

Max Planck–Cardiff Centre on the Fundamentals of Heterogeneous Catalysis FUNCAT, Cardiff Catalysis Institute, School of Chemistry, Cardiff University, Cardiff CF24 4HQ, United Kingdom
E-mail: taylorsh@cardiff.ac.uk

Received 07-11-2024 **Accepted** 08-02-2024 **Published on line** 08-15-2024

Abstract

The gas phase conversion of glycerol to methanol is a complex reaction with numerous side reactions. Herein, a series of MgO materials have been prepared and calcined at a range of temperatures to investigate the influence of calcination temperature on the physicochemical properties of MgO and the subsequent effect on catalytic performance. XRD, N_2-physisorption and TEM were used to explore the properties of the materials, with CO_2 adsorption techniques utilised to investigate the basic properties of the catalysts. Catalyst testing showed that observed carbon balance increased with decreasing basicity, with the "missing" carbon attributed to the formation of high molecular weight products that are not routinely quantified. The formation of high molecular weight products was favoured by hydroxylated MgO surfaces, with the extent of surface hydroxylation relating to the nature of the basic sites. MgO calcined at a temperature of 650 °C exhibited a full carbon balance which was attributed to the low relative proportion of low-coordinate O^{2-} sites, and the associated low degree of surface hydroxylation.

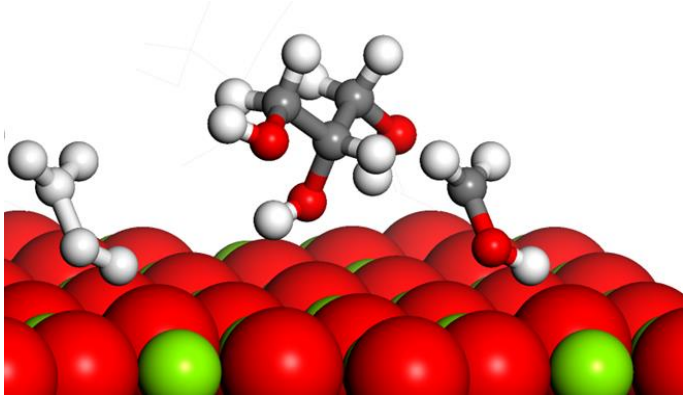

Keywords: Glycerol upgrading, methanol, MgO, Basic site, condensation
Cite as *Arkivoc* **2024** (3) 202412252
DOI: https://doi.org/10.24820/ark.5550190.p012.252

Introduction

In recent decades, there has been an increasing drive for the sustainable production of liquid fuels and chemical products.[1,2] The use of renewable or carbon neutral feedstocks has therefore become an attractive prospect for researchers and as a consequence, much emphasis has been placed on reducing dependency on chemistry with coal, oil or gas as a starting point. As a result, the biodiesel industry has seen growth in recent years, which is projected to continue. The global biodiesel market was valued at $32.1 billion in 2021 and is projected to be worth $73.05 billion by 2030.[3] The majority of biodiesel produced commercially comprises of fatty acid methyl esters (FAMEs), generated through the transesterification of triglycerides. For this process, methanol and a base are commonly employed as a reagent and catalyst, respectively.[4,5] Hydrolysis of the triglycerides results in the formation of glycerol with approximately one ton of glycerol produced for every ten tons of biodiesel,[6] which has ultimately resulted in an oversupply of crude glycerol. As a consequence, glycerol upgrading has become a common goal.[7] While there are many commercial applications for the use of pure glycerol, the purification process is costly, and glycerol produced as a byproduct of biodiesel production typically contains numerous impurities. Hence, there is a collective drive to develop processes and infrastructure that can utilise crude glycerol directly as a feedstock.

In 2015, we initially reported that glycerol could be efficiently transformed into methanol, when vaporized aqueous glycerol solutions are reacted over metal oxide catalysts, such as MgO or CeO_2.[8] This process provides a route for the conversion of glycerol to methanol at atmospheric pressure and without the need for an external reductant. Additionally, the process was also demonstrated with crude glycerol (purity *ca.* 85%), removing the need for extensive purification. Methanol derived from glycerol could provide a number of benefits, not only reducing the oversupply of crude glycerol, but also providing a sustainable route to methanol production. Given that methanol is a reagent in the FAME process, the ability to recycle the glycerol by-product to methanol could provide both environmental and economic advantages to biodiesel producers.

Following the initial report on the process, the valorisation of glycerol to methanol in the vapour phase was the subject of several additional studies.[9-12] One of the primary limitations of the initial work was that the majority of the reactions were conducted with low glycerol concentrations. Upon increasing the concentration of glycerol in the feedstock, reduced methanol space time yields (STYs) were observed, along with a significantly more diverse product distribution. Further investigations with a more concentrated feedstock (50 wt.% aqueous solution) led to a better understanding of the reaction mechanism and dominant reaction pathways which occur, allowing for a more complete reaction scheme to be devised.[13] Despite improvements to the analytical methodology, large quantities of carbon were still unaccounted for in the reaction (25-40% of carbon was missing when a 50 wt.% glycerol feedstock was utilized). This was attributed to the formation of high molecular weight products (HMWPs) *via* bimolecular condensation reactions, which are not quantifiable through our usual analytical techniques. Through identification of the catalytic properties which promote these undesirable reactions, it was hoped that we could design materials to suppress them, which should also lead to increased methanol STY.

Bimolecular condensations are commonly observed in reactions between unsaturated compounds over MgO.[14-19] MgO has been specifically investigated as a catalyst for vapour phase aldol condensation of acetone to form α,β-unsaturated ketones and was found to be an efficient catalyst for the reaction, with activity attributed to the basic properties of the material.[12] Interestingly, these reactions were carried out under similar conditions to those used for the transformation of glycerol to methanol, suggesting that similar reactions may occur in the process.

With this in mind, the goal of this work was to further understand how HMWPs are formed in our glycerol reactions. Specifically, we aim to understand the catalytic properties that promote the formation of HMWPs, so that the space-time-yields of high value target products can be enhanced. Herein, a series of MgO catalysts were prepared under different calcination conditions to study the influence of physicochemical properties in this reaction.

Results and Discussion

It has been reported that thermal treatments used in the preparation of MgO can dramatically influence the basic properties of the material obtained.[15] We aimed to use this approach to produce a set of materials with systematically varying basic character for investigation in the glycerol to methanol reaction. A series of MgO catalysts, prepared using different heat treatment conditions, were synthesised using a method established in our previous work.[8,13] This method involved cycling between hydroxide and oxide phases. Firstly, the starting material $Mg(OH)_2$ was calcined, resulting in the formation of MgO. This material was subsequently dispersed in water, and refluxed for 3 hours at 110 °C, resulting in full rehydration. After drying, the material was exposed to a final thermal treatment under N_2 at a range of temperatures (450-750 °C). This final thermal treatment was included to vary the basicity across the range of samples produced and we will include the temperature of the final thermal treatment when naming samples. Further details of our material preparation is provided in the Experimental section.

A range of characterisation techniques were used to establish how the final heat treatment had actually influenced the physicochemical properties, including the basicity, of each MgO sample.

The BET surface area, total pore volume and average pore diameter for each material are listed in Table 1. Specific surface areas of 187, 154, 125 and 74 $m^2 g^{-1}$ were determined for MgO_450, MgO_550, MgO_650 and MgO_750, respectively, and show that the surface area decreases with increasing temperature in the final step of synthesis. The pore volume followed a similar trend, decreasing with increasing heat treatment temperature. Interestingly, the associated pore radii do not change systematically with heat treatment temperature. The pore radii increased from 18 Å (MgO_450), to the maximum observed value of 118 Å (MgO_550), before decreasing again to 45 Å (MgO_750). These measurements of structural features show that structural differences are induced by differences in the final heat treatment, and this must be considered alongside any changes in basicity.

PXRD patterns of the catalysts were also obtained (Figure 1(a)). Each pattern was indexed to the MgO periclase structure, with no evidence of any residual crystalline $Mg(OH)_2$. There was a notable increase in MgO crystallinity as the heat treatment temperature increased. The crystallite size of each sample was subsequently estimated using the Scherrer equation (Figure 1(b), Table 1) and aligned well with the BET surface areas of the materials (Table 1). The lattice parameter and cell volumes were also determined through further evaluation of the associated diffraction patterns and showed an inverse relationship to MgO crystallite size.

Table 1. Textural, structural and basicity data, derived from N_2 physisorption, XRD and CO_2-TPD experiments for the series of MgO catalysts

Catalyst ID	Heat Treatment[a] / °C	Surface Area[b] / $m^2\ g^{-1}$	Pore Volume[c] / $cm^3\ g^{-1}$	Pore Radius / Å	Crystallite size / nm	CO_2 desorption / $\mu mol\ g^{-1}$	CO_2 desorption / $\mu mol\ m^{-2}$
MgO_450	450	187	0.95	18	6.2	1410	7.54
MgO_550	550	154	0.89	118	7.5	1290	8.38
MgO_650	650	125	0.83	90	8.4	1020	8.16
MgO_750	750	74	0.31	45	12.7	640	8.65

Notes: [a]under flowing N_2. Data acquired through analysis of the materials by interpretation of full N_2 sorption isotherms using [b]BET and [c]BJH methods. Crystallite sizes were estimated using the Scherrer equation, through comparing the FWHM of the MgO (200) reflection with a crystalline silicon standard.

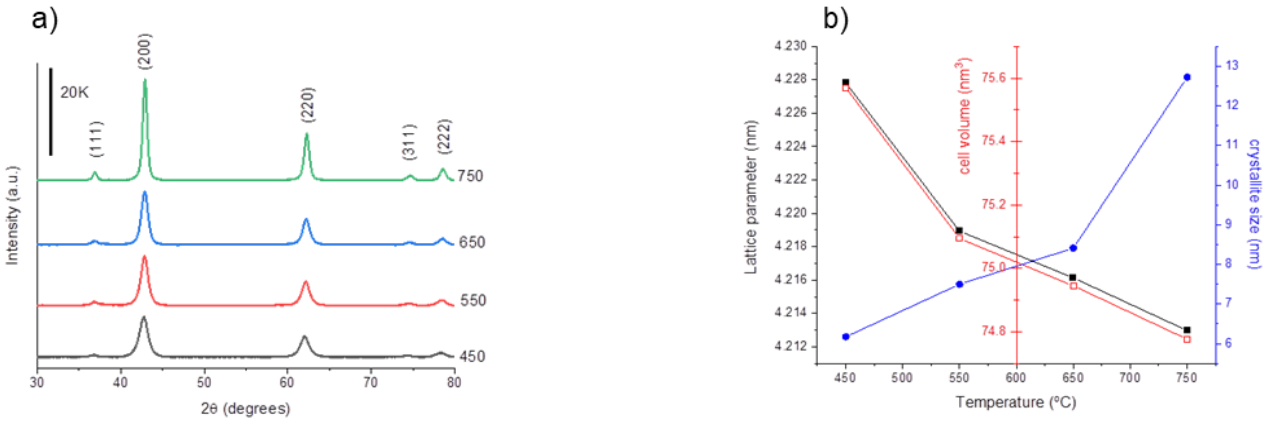

Figure 1. (a) Powder XRD patterns for catalysts MgO_450 (black), MgO_550 (red), MgO_650 (blue), MgO_750 (green). **(b)** based on the (200) reflection: Lattice parameter, cell volume and crystallite size as a function of treatment temperature.

Examination of the materials by TEM (Figure 2) showed notable differences. After thermal treatment at 450 °C, hexagonal MgO platelets were observed (Figures 2(a) and (b)). Previously, Gregory and co-workers demonstrated that well-defined hexagonal platelets of $Mg(OH)_2$ can be synthesised simply through the hydration of MgO with deionised water and that the morphology could be retained upon subsequent dehydration of $Mg(OH)_2$ to MgO by thermal treatment in N_2.[20] Interestingly, increasing the temperature of the inert thermal treatment to 650 °C, resulted in a significant change in the microstructure of the materials (Figure 2 (c) and (d)). Despite maintaining a periclase crystal structure (Figure 1), it is evident that MgO_650 possesses a large proportion of irregular intercrystallite channels. This phenomenon has been observed previously, and is widely recognised to be attributed to the formation and omission of water molecules during the dehydration of $Mg(OH)_2$.[21] After heating the sample to 750 °C, the associated TEM micrographs (Figure 2 (e) and (f)), show that the irregular MgO crystallites have begun to aggregate, leading to the formation of a lamella-like structure. There is some evidence to suggest that the hexagonal crystallites are also beginning to reform.

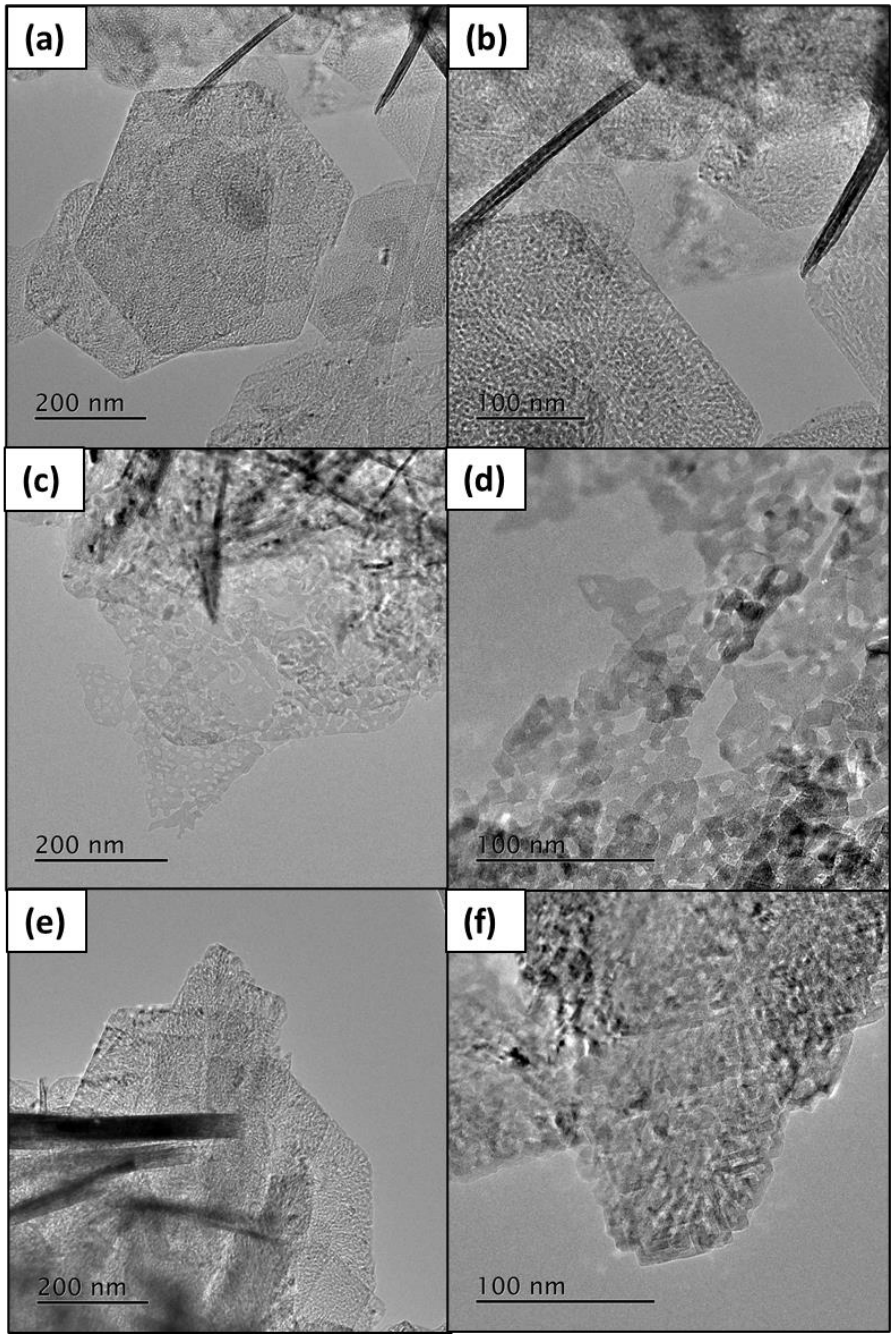

Figure 2. Representative TEM micrographs of the MgO_450 (a) and (b), MgO_650 (c) and (d), MgO_750 (e) and (f) catalysts.

The basic properties of each MgO catalyst were probed by CO_2-TPD and CO_2-DRIFTS. CO_2 can readily adsorb on to MgO, forming a number of different carbonate species, depending on the surface environment. Unidentate carbonate species form when CO_2 reacts with O^{2-} anions,[18] with these low coordinate (high energy) anionic species typically located at edge or corner sites. Bidentate carbonate species are typically formed when CO_2 adsorbs to the oxygen in Mg^{2+}-O^{2-} pairs.[22] Bicarbonate species are formed when CO_2 reacts with surface bound hydroxyl species.[23,24] These species are considered to be fairly labile and are often assigned as weakly basic sites.[25]

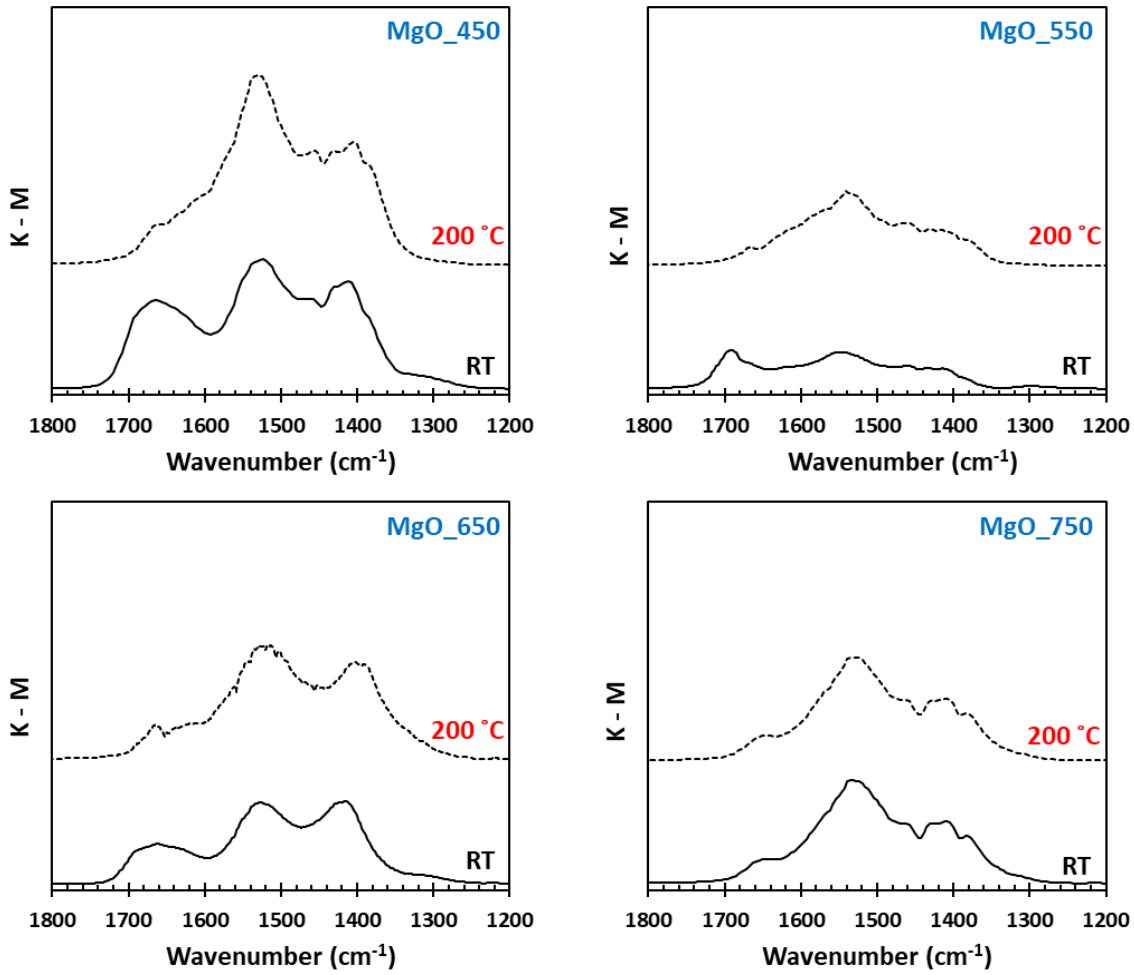

Figure 3. CO_2-DRIFTS spectra for the series of MgO catalysts. Spectra were collected at room temperature and 200 ˚C, after exposure to CO_2. Prior to CO_2 exposure, each sample was subjected to a thermal pre-treatment, involving heating to 450 ˚C under N_2.

The spectra obtained from the CO_2-DRIFTS experiments are presented in Figure 3, with spectra obtained at room temperature and 200 °C for each material. Literature assignments for adsorbed CO_2 on MgO are compiled in Table S2, to aid with assigning the carbonate species observed over the MgO catalysts. The dominant adsorption bands centred at *ca.* 1415 cm^{-1} and 1525 cm^{-1} are characteristic of the symmetric and asymmetric stretching of O-C-O moieties in unidentate magnesium carbonate, respectively.[18] Bidentate carbonate species typically exhibit bands at 1610-1630 cm^{-1} and 1320-1340 cm^{-1}, indicative of asymmetric and symmetric O-C-O stretching, respectively. Bicarbonate species typically exhibit three adsorption bands; symmetric and asymmetric O-C-O stretching (typically observed at *ca.* 1460 cm^{-1} and 1640-1680 cm^{-1}, respectively) and a C-OH bending mode (present at *ca.* 1220 cm^{-1}). There is clear evidence of the asymmetric O-C-O stretch, attributed to bicarbonate species for all samples in the room temperature spectra, although this adsorption mode appears to be comparatively small for MgO_750. After heating to 200 °C, there was a significant reduction in the intensity of the adsorption band at 1640-1680 cm^{-1}. This suggests that the surface bound hydroxyl species, responsible for bicarbonate formation, are likely to be the weakest basic sites in these MgO materials, which is in agreement with previous reports.[25, 26] Interestingly, only a modest reduction in the intensity of the bicarbonate band was observed upon heating at 200 °C for MgO_750, in contrast to the other materials, which may indicate the presence of more stable hydroxyl species for samples synthesised with the highest temperature thermal

treatment. From the spectra it is clear that unidentate carbonate species were formed across all materials, suggesting low coordinate O^{2-} sites are present in all samples, albeit with varying amounts. Similarly, adsorption bands attributed to bicarbonate species were observed over all four materials, with varying relative intensities, suggesting differing degrees of surface hydroxylation.

CO_2-TPD experiments (Figure 4) were performed to better understand the strength of the basic sites on these catalysts and their surface concentrations through quantification of CO_2 desorption (Table 1). The amount of CO_2 desorbed decreased as the thermal treatment temperature increased, indicating a reduction of the total basicity (per gram) of the materials. However, the CO_2 desorption normalised to surface area is within 10 % of the average value of 8.18 µmol m^{-2}, for all samples. This indicates that the surface density of basic sites is practically independent of the synthesis calcination temperature. The findings from the CO_2-DRIFTS experiments, along with reference to previous literature, suggests that each of the TPD traces would be expected to have three primary peaks, representing unidentate carbonate, bidentate carbonate and bicarbonate species.[18,25,27,28] However due to the complexity of the TPD profile, full peak deconvolution and quantification was not achieved. The peak centred at *ca.* 190 °C is attributed to bicarbonate species formed with surface hydroxyl species, which is known to be the lowest basic strength site present in MgO, referred to as weak sites. The signal centred at *ca.* 320 °C has been assigned to the decomposition of unidentate carbonate species, formed on isolated O^{2-} sites, these are strong base sites, while the signal centred at *ca.* 240 °C has been assigned to bidentate species, formed on Lewis acid-Brønsted base pair sites (Mg^{2+}-O^{2}), which are moderate base sites.

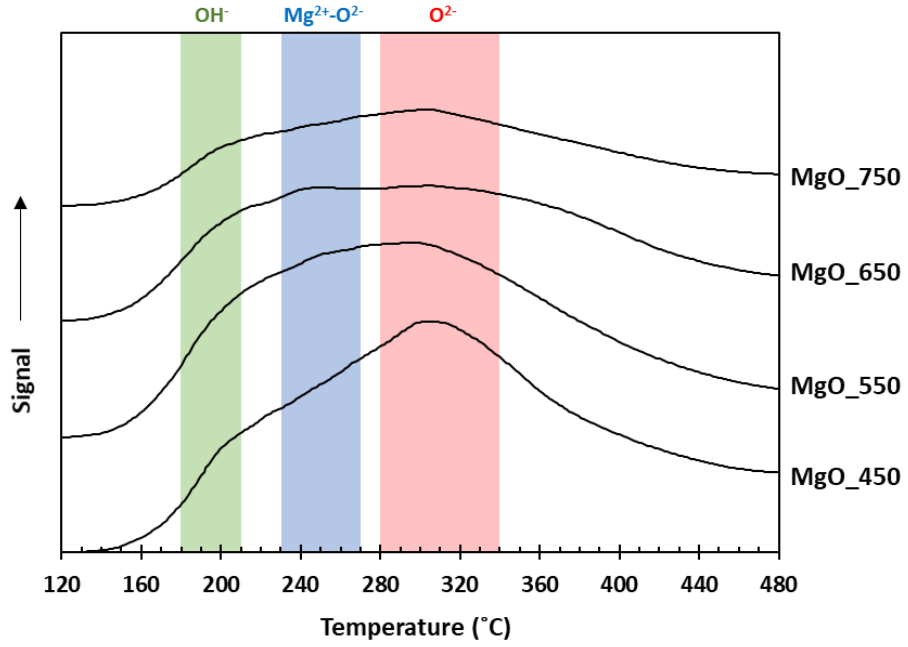

Figure 4. CO_2-TPD profiles for the series of MgO catalysts. Prior to CO_2 exposure, each sample was subjected to a thermal pre-treatment, involving heating to 450 ˚C under N_2.

In addition to possessing the highest total basicity, MgO_450 has the highest proportion of strongly basic O^{2-} sites, represented by unidentate carbonate formation. Interestingly, the proportion of O^{2-} sites appears to decrease as the calcination temperature is increased from 450 to 650 °C, although O^{2-} site proportion then increases as the calcination temperature is further increased to 750 °C, so that MgO_650 has the lowest proportion of O^{2-} sites. Overall, MgO_650 also has a higher proportion of weak (OH^-) and medium strength basic

sites (Mg^{2+}-O^{2-}) sites than the other samples, which have a higher proportion of strongly basic sites (O^{2-}). Despite the clear differences in the basic character of the samples prepare with different calcination temperatures we were unable to identify any systematic link between the microstructure information from XRD and TEM and the range of basic site types evidenced by CO_2-TPD and CO_2-DRIFTS.

Glycerol Conversion over MgO Catalysts

The MgO materials synthesised in this work were investigated as catalysts for the gas-phase conversion of glycerol. For consistency, the testing conditions used were comparable to those which we have used previously,[11, 13] with 50 wt.% aqueous glycerol at 360 °C in an inert gas flow. The results from these experiments are presented in Table 2.

The activity of the catalysts can be tentatively correlated to the pre-treatment temperature. As the pre-treatment temperature increases, glycerol conversion (C_{gly} (%)) decreases from MgO_450 to MgO_650, reflected in the activity (g_{gly} h^{-1} g_{cat}^{-1}). The reduction in conversion with increasing heat treatment temperature correlates well to the decreasing surface area. However, despite the low surface area and total basicity, MgO_750 exhibited higher activity than MgO_650 and MgO_550, suggesting an additional factor may be responsible for the increased activity of this catalyst. Considering the CO_2-TPD and DRIFTS experiments, increase in activity for MgO_750 is likely related to a higher proportion of strongly basic low coordinate O^{2-} sites.

Table 2. Performance of MgO catalysts on the gas phase valorisation of glycerol

Catalyst ID	C_{gly} / %	% Selectivity (**STY** / g h^{-1} kg_{cat}^{-1})												coke* /mg g_{cat}^{-1}	CMB / %	Coke / % of CMB
		ACE		ACR		MOH		HAD		EG		UNK				
MgO_450	87	20	(**92**)	13	**(53)**	12	(**85**)	23	(**122**)	8	(**54**)	8	(**NA**)	89.1	74	3.0
MgO_550	80	17	(**83**)	11	**(45)**	10	(**74**)	28	(**152**)	9	(**63**)	8	(**NA**)	79.2	78	2.9
MgO_650	75	20	(**118**)	13	**(64)**	10	(**93**)	24	(**173**)	9	(**71**)	8	(**NA**)	105.5	98	3.2
MgO_750	80	22	(**98**)	13	**(49)**	11	(**79**)	23	(**122**)	8	**(52)**	8	(**NA**)	43.5	79	2.1

Reaction conditions: Aqueous glycerol solution (50 wt.%; 0.016 mL min^{-1}; Ar(50 mL min^{-1}); catalyst (0.5 g); bed volume (1 mL); GHSV = 3000 h^{-1}; temperature (360 °C).

Abbreviations: C (conversion); ACE (acetaldehyde), ACR (acrolein); MOH (methanol); HAD (hydroxyacetone); UNK (unknown); EG (ethylene glycol); CMB (carbon mass balance: ratio of GC1 + GC2 reaction products + coke carbon moles to carbon moles of glycerol injected into reactor).

*Coke as deposited carbon on the catalyst surface, calculated from mass loss in TGA

There were no significant differences in observed product selectivity (as carbon mol. selectivity) across the catalysts, but notable differences in carbon mass balance were found, reflected by differences in product STYs. As product quantification was conducted by gas chromatography, the presence of HMWPs are undetected and thus unquantifiable, due to their lack of volatility. However, the selectivity to HMWPs can be inferred from the carbon balance. A higher carbon balance would correspond to a lower selectivity to HMWPs. The carbon balance was 98% over MgO_650, indicating a low selectivity to HMWPs. LCMS analysis of the post-reaction mixture obtained over MgO_650 and MgO_450, suggested a higher degree of HMWPs for the MgO_450 liquid product fraction than MgO_650 (Figure S3), which correlates with the observed carbon balance. While the selectivity to

methanol did not increase over MgO_650, a modest increase in STY was observed for all major detectable products. For instance, a higher methanol space time yield of 93 g h^{-1} kg cat h^{-1} was observed over the MgO_650 catalyst, compared to 85 g h^{-1} kg cat h^{-1} over MgO_450, despite the lower glycerol conversion over MgO_650.

Analysis of the total carbon content of the liquid fraction of a reaction mixture formed over MgO_650 by CHN analysis (Table S5) was in good agreement with GC analysis of the liquid products at 85%. The remaining carbon was assigned to coking (3.2%), determined by TGA, and gas phase products (8.7%), confirming that only a small amount of carbon, if any, was present in the form of HMWPs.

Figure 5 presents a proposed scheme for the catalytic formation of HMWPs over MgO. Here, a cross-condensation reaction between acetone and acetaldehyde is used as an example. This leads to four different products as there are two possibilities of enolate nucleophiles and carbonyl electrophile. Self-condensation, which likely occurs with acetone would result in an α,β-unsaturated ketone. Based on a classical understanding of the aldol condensation mechanism the reactions are catalysed by the MgO basic site abstracting an α-proton from a methyl group of a ketone or aldehyde which results in the formation of an enolate.[19] This enolate then acts as a nucleophile with the electron rich carbon in the enolate attacking on the keto-carbon of a second molecule. This is followed by protonation to yield the aldol addition product. This product can then undergo a catalytic elimination of water produced from the α-hydrogen and the β-hydroxyl group resulting in an enone.

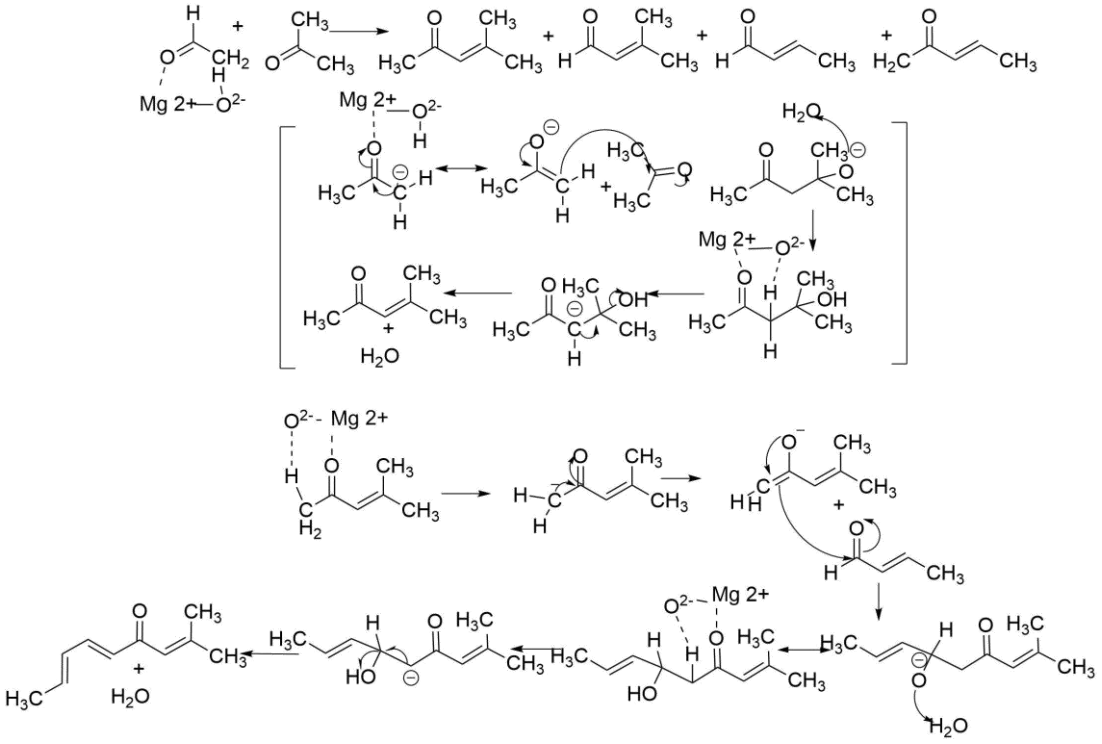

Figure 5. Aldol cross-condensation of acetone and acetaldehyde. Followed by possible cross-condensation of α,β-unsaturated ketone (acetone enolate) and acetaldehyde enolate to form HMWP's.

Another common route would be self-condensation of acetaldehyde to 3-hydroxybutanal, which in turn can undergo a dehydration of acid sites to crotonaldehyde. Subsequent reactions of these products *via* routes such as Michael additions, dehydrations, electrocyclization and aldol condensations could lead to larger products and aromatic products such as benzene and tolualdehydes.[29] Products postulated and determined in other work

include *ortho*- and *para*-tolualdehyde, 2,4,6-octatrienal and 2,4-hexadienal.[30-32] These larger products could result in further additions resulting in the HMWPs with higher masses and expected high boiling points.

There are also reported instances of hydroxyl species on MgO surfaces being active for certain base catalysed reactions.[28,33] Zhang *et al.,* found that the hydroxyl species were the active sites for the aldol addition of acetone, with the addition of water to a clean MgO surface leading to a significant increase in both activity and selectivity to diacetone alcohol.[34] DFT studies performed by Fan *et al.*[19] highlighted the role of hydroxyl species in acetaldehyde condensation, which is a major product in our product stream. A significant reduction in the activation energy of the reaction was calculated in the presence of water, attributed to both surface hydroxylation and the ability of water to participate in the reaction through protonation of the alkoxide ion. Figure 6 shows how the self-condensation of acetaldehyde can occur over partially hydroxylated MgO surfaces. As described above, subsequent reactions of 3-hydroxybutanal or crotonaldehyde can occur leading to the formation of HMWPs, thus acetaldehyde coupling can lead to a reduction in observed carbon balance.

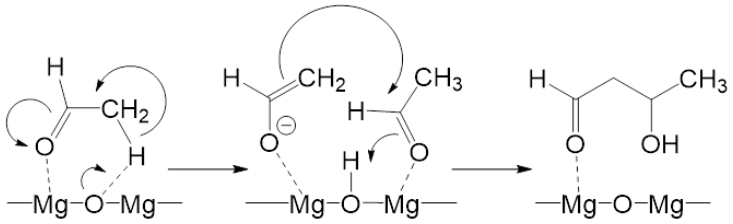

Figure 6. Acetaldehyde self-condensation to hydroxybutanal over a partially hydroxylated surface, in accordance with DFT calculations from Fan *et al.*[19]

Both the DRIFTS and TPD experiments in our work show that a variety of basic sites are present in the MgO catalysts. MgO_650 possesses the lowest relative proportion of strongly basic sites, represented by unidentate carbonate formation on isolated O^{2-} sites. Since water is present in the reactant stream, hydroxylation of the MgO surface is likely to occur. It is hypothesized that the lower proportion of strongly basic sites present in MgO_650 leads to a reduction in the degree of surface hydroxylation, reducing the extent of high HMWP formation. A lower degree of surface hydroxylation could also explain the reduced glycerol conversion obtained over MgO_650 (75%) compared with MgO_750 (80%), despite the significantly higher surface area (125 *vs.* 74 $m^2\ g^{-1}$). Whilst MgO_750 possesses the lowest total basicity, it has a relatively high proportion of strongly basic sites which are likely hydroxylated, promoting HMWP formation.

The role of surface hydroxylation on product distribution was investigated by replacing the H_2O solvent with D_2O over MgO_450, MgO_550 and MgO_650 (Tables S7-9). Replacing the H_2O solvent with D_2O resulted in a reduction in glycerol conversion the level of reduction followed the trend MgO_450 > MgO_550 > MgO_650, with conversion decreasing from 87 to 54% over MgO_450 and from 80 to 53% over MgO_550. Conversely, replacing H_2O with D_2O led to a much more modest reduction in glycerol conversion over MgO_650, from 75 to 71%. Interestingly, with a D_2O solvent, full carbon balances were obtained over both MgO_450 and MgO_550, suggesting that HMWP formation was suppressed over these materials in the presence of D_2O, which is in agreement with previous reports,[34,19] and further highlights the role of surface hydroxylation.

The high carbon balance for MgO_650 using both H_2O and D_2O solvents sparked our interest in this catalyst when first highlighted due to the associated increase in space-time-yield for desired products such as methanol, and other platform chemicals. Experiments using hydroxyacetone, instead of glycerol were performed over MgO_650 and MgO_450 at 320 and 360 °C. As shown in Table S10, a modest hydroxyacetone conversion (16%) was achieved over MgO_450, in contrast to MgO_650 which showed negligible activity under these conditions.

In addition to being a major by-product in the conversion of glycerol to methanol, hydroxyacetone contains both ketone and alcohol functional groups with the ability to undergo condensation reactions. The limited ability of MgO_650 to convert hydroxyacetone is indicative of its limited propensity for HMWP formation. Both acetaldehyde and hydroxyacetone, major products in this process, have been reported to undergo condensation reactions over basic catalysts,[35,36] therefore, minimising these reactions is crucial to achieving high carbon balances and space-time-yields. From a practical perspective, reducing the presence of HMWPs in the product stream is highly desirable - HMWPs often have higher boiling points leading to product condensation, ultimately resulting in catalyst deactivation and in reactor fouling requiring increased reactor maintenance.

Conclusions

MgO catalysts were prepared by varying the calcination temperature between 450 – 750 °C and evaluated for the gas phase conversion of glycerol. As the calcination temperature increased, the total basicity of the materials decreased. As the calcination temperature was increased up to 650 °C the density of strongly basic sites, attributed to low coordinate O^{2-} anions, decreased, although the proportion of these strong sites increased upon further increasing the calcination temperature to 750 °C. Glycerol conversion was found to follow the same trend as strongly basic site distribution with conversion decreasing as the calcination temperature is increased from 450 to 650 °C, with a slight increase in conversion for the catalyst calcined at 750 °C. The observed carbon balance followed an inverse trend to glycerol conversion, with the highest observed carbon balance achieved over MgO_650. The loss of carbon is attributed to the presence of bimolecular condensation reactions which form HMWPs that are not routinely quantified in our analysis. Condensation reactions are known to be promoted by hydroxylated MgO surfaces, and so we suggest that the degree of surface hydroxylation under reaction conditions correlates to the loss of observed carbon. Reactions performed with D_2O agreed with this hypothesis, and full carbon balances were obtained when the H_2O solvent was replaced with D_2O. The full carbon balance achieved over MgO_650 suggested the minimal formation of HMWPs and is a significant step forwards in closing the gap in observed carbon balance. Whilst moderate increases in space-time-yields to desired products such as acetaldehyde, methanol and ethylene glycol were observed over MgO_650 due to the reduced formation of HMWPs, there were no significant differences in observed product selectivity. Further investigations on the nature of MgO surface hydroxylation should contribute to future work, with the aim of minimising HMWP formation and simultaneously maximising methanol selectivity.

Experimental Section

General. Acetaldehyde (> 99.5%), acrolein (≥ 99%) cyclohexanol (99%), ethylene glycol (≥ 99%) glycerol (≥ 99.5%), hydroxyacetone (≥ 90.0%), magnesium (II) hydroxide (≥ 99.0%), and methanol (≥ 99.9%) were all purchased from Merck. Argon and acetaldehyde in helium (1000 ppm) was supplied by BOC. All purchased materials were used as received unless otherwise specified. Deionised water was provided in-house. Silicon carbide (98%, Alfa Aesar, 40–50 mesh size) was washed with deionised water and dried prior to use (110 °C, 24 h).

Catalyst preparation. MgO catalyst samples were prepared following a previously established procedure,[8,9] using commercially available $Mg(OH)_2$ as a starting material. For all samples, $Mg(OH)_2$ was first calcined in a

tubular Carbolite furnace at 450 °C in static air for 2 h (10 °C min^{-1}). The solid obtained was subsequently refluxed in water (15 mL g^{-1}) for 3 h at 110 °C, before the resulting slurry was dried in an oven at 90 °C for 24 h. The samples were then heat treated at; 450 °C, 550 °C, 650 °C or 750 °C (ramp rate from ambient of 10 °C min^{-1}) for 3 h under N_2 flow. These materials are denoted as MgO_450, MgO_550, MgO_650 and MgO_750, respectively.

Characterisation. Powder X-ray diffraction (XRD) was conducted using a PANalytical X'Pert Pro system fitted with a CuK_α X-ray source operated at 40 kV and 40 mA. Each sample was scanned over a 2θ range of 10° to 80° with a step size of 0.016°. Surface area and porosity measurements were determined by N_2 adsorption with 20-point adsorption, 20-point desorption isotherms performed at 77 K on a Quadrasorb evo™ Gas Sorption Surface Area and Pore Size Analyser. Prior to the analysis, samples (*ca.* 100 mg) were degassed at 220 °C for 3 h, under vacuum.

CO_2 temperature programmed desorption (CO_2-TPD) was carried out on a Quantachrome ChemBET instrument. Typically, the sample (*ca.* 100mg, 300 - 425 mesh) was pre-treated at 400 °C (15 °C min^{-1}) for 1 hour under flowing He (80 mL min^{-1}). CO_2 was subsequently passed over the material at room temperature for 20 minutes. Physisorbed CO_2 was removed by heating to 110 °C (15 °C min^{-1}) under flowing He (80 mL min^{-1}) and holding for 1 hour. Chemisorbed CO_2 was desorbed by heating to 1100 ^{0}C (15 °C min^{-1}) under flowing He (80 mL min^{-1}). Desorbed CO_2 was monitored and quantified by TCD. CO_2-DRIFTS measurements were carried out using a Brüker DRIFT tensor 27 FTIR spectrometer fitted with a mercury cadmium telluride (MCT) detector. DRIFT spectra were recorded in the 4000-1000 cm^{-1} range using a spectral resolution of 6 cm^{-1} (64 scans/spectrum) using a Praying Mantis high-temperature cell with KBr windows. Samples were pre-treated in-situ at 400 °C for 2 hours in flowing nitrogen (18 mL min^{-1}) Background spectra were recorded at 400 °C, 300 °C, 200 °C, 100 °C and room temperature. CO_2 was flowed over the sample (3 mL min^{-1}) in nitrogen (18 mL min^{-1}) for 20 minutes until the surface was saturated. Spectra were obtained at room temperature, 100 °C, 200 °C, 300 °C and 400 °C.

Transmission electron microscopy (TEM) was performed on a JEOL JEM-2100 microscope operating at 200 kV. Samples were prepared by dispersion in ethanol by sonication and deposited on 300 mesh copper grids coated with holey carbon film.

Catalyst testing. Catalysts were pelleted, crushed, and sieved to a uniform particle size (300–425 µm) prior to testing. Reaction testing set up and the subsequent instrumental analysis of the product mixture *via* GC and LCMS was carried out in line with instrumentation method presented in Smith *et al.*[9]

Briefly, 0.5 g of pelleted catalyst was made up to 1 mL with a SiC diluent and packed into an 8 mm inner diameter stainless-steel tube between plugs of quartz wool, corresponding to a GHSV of 3000 h^{-1}. For the initial 2 hours and 15 minutes on stream, the reaction mixture was diverted to waste to ensure a steady flow of glycerol throughout the reactor; after this time, liquid products were condensed and collected in a stainless-steel trap submerged in an ice-bath while vapor phase products were collected in an attached gas bag.

Glycerol conversion, product selectivity, carbon balance and space time yield were calculated in accordance with the equations provided in the ESI. Total selectivity to unknown products was quantified using the cumulative peak area of the unidentified GC chromatogram peaks, assuming an average of 3 carbon atoms in unknown products; the approximate response factor was based on the average of the response factors for detected products. CHN analysis was performed externally by Exeter Analytical UK Ltd. to establish total organic carbon content.

Carbon deposition following a catalytic reaction was estimated by thermal gravimetric analysis (TGA) and differential thermal analysis (DTA), performed on a Setaram Labsys 1600 instrument. Samples (20-70 mg) were loaded into alumina crucibles and heated to 800 °C (5 °C min^{-1}) in a flow of synthetic air (50 mL min^{-1}).

Acknowledgements

We would like to thank the EPSRC for funding this work (Grant reference code: EP/P033695/1). The authors would also like to thank Exeter Analytical UK Ltd. for the Total Organic Content analysis. We would also like to acknowledge Thomas Williams for assistance with the operation of and processing of the LC-MS data. We would like to thank the Cardiff University electron microscopy facility for the TEM imaging. We thank the Max Planck Society and the Cardiff University for financial support to create the FUNCAT Centre.

Supplementary Material

The supplementary information contains XRD patterns and crystallite sizes of commercial $Mg(OH)_2$ and after rehydration; TGA of $Mg(OH)_2$ dehydration; literature assignments for CO_2 adsorption; full product list and analysis; LC-MS chromatograms; CHN analysis; product distributions for a range of conditions. Information on the data underpinning the results presented here can be found in the Cardiff University data catalogue at http://doi.org/10.17035/d.2024.0322858194.

References

1. Alonso, D. M.; Bond, J. Q.; Dumesic, J. A. *Green Chem.* **2010**, *12*, 1493-1513. https://doi.org/10.1039/c004654j
2. Sudarsanam, P.; Zhong, R.; Van den Bosch, S.; Coman, S. M.; Parvulescu, V. I.; Sels, B. F. *Chem. Soc. Rev.* **2018**, *47*, 8349-8402. http://dx.doi.org/10.1039/C8CS00410B
3. *Biodiesel Market Size, Share & Trends Analysis Report By Feedstock (Vegetable Oils, Animal Fats), By Application (Fuel, Power Generation), By Region (Europe, APAC), And Segment Forecast*, Report GVR-1-68038-513-7, Grand View Research, 2021.
4. Lotero, E.; Liu, Y.: Lopez, D. E.; Suwannakarn, K.; Bruce, D. A.; Goodwin, J. G. *Ind. Eng. Chem. Res.* **2005**, *44*, 5353-5363. https://doi.org/10.1021/ie049157g
5. López, D. E.; Goodwin, J. G.; Bruce, D. A. *J. Catal.*, **2007**, *245*, 381-391. https://doi.org/10.1016/j.jcat.2006.10.027
6. Pagliaro, M.; Rossi, M. in *The Future of Glycerol*, The Royal Society of Chemistry, **2010**, p. 1-28. https://doi.org/10.1039/9781849731089
7. Pagliaro, M.; Ciriminna, R.; Kimura, H.; Rossi, M.; Della Pina, C. *Angew. Chem. Int. Ed.*, **2007**, *46*, 4434-4440. https://doi.org/10.1002/anie.200604694
8. Haider, M. H.; Dummer, N. F.; Knight, D. W.; Jenkins, R. L.; Howard, M.; Moulijn, J.; Taylor, S. H.; Hutchings, G. J. *Nat. Chem.*, **2015**, *7*, 1028-1032. https://doi.org/10.1038/nchem.2345
9. Devlia, J.; Smith, L.; Douthwaite, M.; Taylor, S. H.; Willock, D. J.; Hutchings, G. J.; Dummer, N. F. *Philos. Trans. R. Soc., A*, **2020**, *378*, 20200059. https://doi.org/10.1098/rsta.2020.0059

10. Sainna, M. A.; Nanavati, S.; Black, C.; Smith, L.; Mugford, K.; Jenkins, H.; Douthwaite, M.; Dummer, N. F.; Catlow, C. R. A.; Hutchings, G. J.; Taylor, S. H.; Logsdail A. J.; Willock, D. J. *Faraday Discuss.*, **2021**, *229*, 108-130. https://doi.org/10.1039/D0FD00005A
11. Smith, L. R.; Sainna, M. A.; Douthwaite, M.; Davies, T. E.; Dummer, N. F.; Willock, D. J.; Knight, D. W.; Catlow, C. R. A.; Taylor, S. H.; Hutchings, G. J. *ACS Catal.*, **2021**, *11*, 4893-4907. https://doi.org/10.1021/acscatal.0c05606
12. Smith, P. J.; Smith, L.; Dummer, N. F.; Douthwaite, M.; Willock, D. J.; Howard, M.; Knight, D. W.; Taylor, S. H. ; Hutchings, G. J. *Energies*, **2019**, *12*, 1359. https://doi.org/10.3390/en12071359
13. Smith, L. R.; Smith, P. J.; Mugford, K. S.; Douthwaite, M.; Dummer, N. F.; Willock, D. J.; Howard, M.; Knight, D. W.; Taylor, S. H. ; Hutchings, G. J. *Catal. Sci. Technol.*, **2019**, *9*, 1464-1475. https://doi.org/10.1039/C8CY02214C
14. Xu, C.; Bartley, J. K.; Enache, D. I.; Knight, D. W.; Hutchings, G. J. *Synthesis*, **2005**, *2005*, 3468-3476. https://doi.org/10.1055/s-2005-918467
15. Di Cosimo, J. I.; Díez, V. K.; Apesteguía, C. R. *Appl. Catal., A,* **1996**, *137*, 149-166. https://doi.org/10.1016/0926-860X(95)00289-8
16. Díez, V. K.; Apesteguía, C. R., Di Cosimo, J. I. *J. Catal.* **2006**, *240*, 235-244. https://doi.org/10.1016/j.jcat.2006.04.003
17. Alghamdi, K.; Hargreaves, J. S. J.; Jackson, S. D. in *Metal Oxide Catalysis*, **2008**, pp. 819-843. https://doi.org/10.1002/9783527626113.ch21
18. Di Cosimo, J. I.; Díez, V. K.; Ferretti, C.; Apesteguía, C. R. in *Catalysis: Volume 26*, eds. Spivey, J.; Dooley, K. M.; Han, Y.-F. The Royal Society of Chemistry, **2014**, vol. 26, p. 1. https://doi.org/10.1039/9781782620037-00001
19. Fan, D.; Dong, X.; Yu, Y.; Zhang, M. *Phys. Chem. Chem. Phys.*, **2017**, *19*, 25671-25682. https://doi.org/10.1039/C7CP04502F
20. Hanlon, J. M.; Bravo Diaz, L.; Balducci, G.; Stobbs, B. A.; Bielewski, M.; Chung, P.; MacLaren, I.; Gregory, D. H. *CrystEngComm*, **2015**, *17*, 5672-5679. https://doi.org/10.1039/C5CE00595G
21. Ding, Y.; Zhang, G.; Wu, H.; Hai, B.; Wang, L.; Qian, Y. *Chem. Mate*r. **2001**, *13*, 435-440. https://doi.org/10.1021/cm000607e
22. Fu, Y.; Zhang, L.; Yue, B.; Chen, X.; He, H. *J. Phys. Chem. C*, **2018**, *122*, 24094-24102. https://doi.org/10.1021/acs.jpcc.8b06827
23. Evans, J. V.; Whateley, T. L. *Trans. Faraday Soc.* **1967**, *63*, 2769-2777. https://doi.org/10.1039/tf9676302769
24. Stark, J. V.; Park, D. G.; Lagadic, I.; Klabunde, K. J. *Chem. Mater.* **1996**, *8*, 1904-1912. https://doi.org/10.1021/cm950583p
25. Menezes, A. O.; Silva, P. S.; Padrón Hernández, E.; Borges, L. E. P.; Fraga, M. A. *Langmuir*, **2010**, *26*, 3382-3387. https://doi.org/10.1021/la903149y
26. Ranjit, K. T.; Klabunde, K. J. *Chem. Mater.* **2005**, *17*, 65-73. https://doi.org/10.1021/cm040360b
27. Díez, V. K.; Ferretti, C. A.; Torresi, P. A.; Apesteguía, C. R.; Di Cosimo, J. I. *Catal. Today*, **2011**, *173*, 21-27. https://doi.org/10.1016/j.cattod.2011.02.060

28. Petitjean, H.; Guesmi, H.; Lauron-Pernot, H.; Costentin, G.; Loffreda, D.; Sautet, P.; Delbecq, F. *ACS Catalysis*, **2014**, *4*, 4004-4014. https://doi.org/10.1021/cs5010807
29. Kurokawa, H.; Yanai, M.; Ohshima, M.-a.; Miura, H. *React. Kinet. Mech. Catal.*, **2012**, *105*, 401-412. https://doi.org/10.1007/s11144-011-0381-5
30. Moteki, T.; Rowley, A. T.; Bregante, D. T.; Flaherty, D. W. *ChemCatChem*, **2017**, *9*, 1921-1929. https://doi.org/10.1002/cctc.201700151
31. Chang, Y.-C.; Ko, A.-N. *Appl. Catal. A*, **2000**, *190*, 149-155. https://doi.org/10.1016/S0926-860X(99)00293-8
32. Lusardi, M. ; Struble, T.; Teixeira, A. R.; Jensen, K. F. *Catal. Sci. Technol.* **2020**, *10*, 536-548. https://doi.org/10.1039/C9CY01927H
33. Chizallet, C.; Costentin, G.; Lauron-Pernot, H.; Krafft, J. M.; Bazin, P.; Saussey, J.; Delbecq, F.; Sautet, P.; Che, M. *Oil Gas Sci. Technol. - Rev. IFP*, **2006**, *61*, 479-488. https://doi.org/10.2516/ogst:2006023a
34. Zhang, G.; Hattori, H.; Tanabe, K. *Appl. Catal.* **1988**, *36*, 189-197. https://doi.org/10.1016/S0166-9834(00)80114-1
35. Quesada, J.; Faba, L.; Díaz, E.; Ordóñez, S. *Appl. Catal. A*, **2017**, *542*, 271-281. https://doi.org/10.1016/j.apcata.2017.06.001

